RESEARCH PAPER

Biomimetic chitosan/alginate with zinc and strontium hydroxyapatite for periodontal regeneration application

Munusamy Suresh[1, 2], Palanisamy Karthikeyan[3], Sriram Kaliamoorthy[4], Pullar Vadivel[5*]

[1]Department of Chemistry, Sri Sarada Niketan College of Arts and Science for women, Salem, India
[2]Department of Chemistry, Periyar University, Salem, India
[3]Department of Chemistry, Government Arts and Science College Idappadi, Salem, India
[4]Vinayaka Mission's Medical College and Hospital, Vinayaka Mission's Research Foundation (Deemed to be University), Karaikal, Puducherry, India
[5]Department of Chemistry, Salem Sowdeswari College, Salem, India.

ABSTRACT

Objective(s): To evaluate the potential of a novel alginate/chitosan/Zinc-strontium hydroxyapatite (AG/CS/SHA) composite scaffold for periodontal tissue regeneration by assessing its biocompatibility, bioactivity, and degradation characteristics.

Materials and Methods: An AG/CS/SHA composite scaffold was fabricated using a freeze-drying technique. Characterization involved Fourier Transform Infrared Spectroscopy (FTIR) to confirm chemical composition, X-ray Diffraction (XRD) to analyze crystallinity, Scanning Electron Microscopy (SEM) and Transmission Electron Microscopy (TEM) to investigate microstructure and surface morphology. In vitro studies assessed biocompatibility using the 3-(4,5-dimethylthiazol-2-yl)-2,5-diphenyltetrazolium bromide (MTT) assay, cell viability with Acridine Orange/Propidium Iodide (AO/PI) staining, alkaline phosphatase (ALP) activity, and calcium deposition to evaluate osteogenic differentiation.

Results: FTIR and XRD confirmed SHA incorporation. SEM/TEM revealed a porous structure with uniform SHA distribution. The composite exhibited controlled swelling and degradation. MTT assay and AO/PI staining demonstrated good cell viability. ALP activity (20% higher) and ARS staining (35% increase) were significantly higher in Zn and Sr in HA within AG/CS (AG/CS/SHA) scaffolds compared to AG/CS (control), indicating enhanced osteogenic differentiation and mineralization.

Conclusion: The results demonstrate that the AG/CS/SHA composite possesses favorable characteristics for bone tissue engineering applications, including excellent biocompatibility, suitable mechanical properties, and the ability to promote osteogenic differentiation. These findings suggest that the AG/CS/SHA scaffold holds significant promise as a promising biomaterial for periodontal tissue regeneration, providing a supportive environment for cell growth, differentiation, and new tissue formation.

Keywords: *Periodontal regeneration, Biocomposites, Hydroxyapatites, Tissue engineering, Osteogenesis*

How to cite this article
Suresh M, Karthikeyan P, Kaliamoorthy S, Vadivel P. Biomimetic chitosan/alginate with zinc and strontium hydroxyapatite for periodontal regeneration application. Nanomed J. 2026;13(1): 170-182. DOI: 10.22038/NMJ.2025.84635.2133

INTRODUCTION

Periodontitis is one of the most common dental illnesses, and it is defined by the deterioration of periodontal tissues, which leads to tooth loosening and possibly tooth loss [1]. Periodontal therapy can reduce chronic inflammation and swelling while also slowing disease development. Periodontal problems, on the other hand, were difficult to restore to their natural structure and function. As a result, numerous studies have focused on the use of bioengineering techniques to accomplish periodontal rejuvenation, which consists of three key components: scaffolds, seed cells, and chemokines [2]. A permeable structure is a type of nanomaterial with pore diameters ranging from 2 to 100 nm that has gained popularity in recent years due to its well-ordered channel system, pore volume, and large interfacial area. Scaffolds with pores can load more signaling molecules and increase bioactivity and cell adhesion.

In periodontal tissue regeneration, hydroxyapatite (HA) is recognized as one of the best scaffolds. It has high cytocompatibility and bioactive characteristics due to its resemblance to the elemental composition of bones [3]. To enhance the

* *Corresponding author:* Pullar Vadivel, Associate Professor, Department of Chemistry, Salem Sowdeswari college, Salem 636010, India. Phone: +91 9994655397, E-Mail address: vadivelsalem@gmail.com.
Note. This manuscript was submitted on December 11, 2024; approved on March 02, 2025.

physicochemical and biological properties of hydroxyapatite, such as mechanical characteristics, osseointegration potential, implant placement efficacy, antimicrobial activities, and degradation rate, by modifying hydroxyapatite composition through small quantities of ions co-doped, which are traced in human bones, minerals such as barium, silicon, magnesium, strontium, and zinc intrigued the interest of researchers [4].

Recent studies have highlighted the advantages of ion substitution in hydroxyapatite (HA) for enhancing its properties in bone regeneration. Strontium (Sr) and zinc (Zn) have emerged as particularly promising substituents due to their unique contributions to bone health. Sr, with its chemical similarity to calcium, has been shown to promote bone formation and reduce bone resorption, making it valuable in treating osteoporosis and improving implant osseointegration [5]. Zn, on the other hand, plays a crucial role in collagen synthesis and mineralization, contributing to increased bone density and strength [6]. Additionally, Zn exhibits antibacterial properties, reducing the risk of implant-associated infections [7]. The combined use of Sr and Zn in substituted HA has shown synergistic effects, improving both the mechanical properties and biological activity of the material [8]. These findings underscore the potential of Sr and Zn co-doped HA as a promising material for bone regeneration applications.

Moreover, it has been proposed that zinc (Zn) and strontium (Sr) co-doping produce significantly better outcomes than single-element doping. Candidates for optimizing osteoconductivity by promoting new human bone formation and encouraging osteoinductivity include Zn and Sr-substituted apatite. So, the ability of Zn and Sr to break down and form bone works together to improve interfacial adhesion, fatigue strength, and the implant's ability to change into a periodontal ligament [9].

Despite their advantages, substituted hydroxyapatites (SHA) have limits in mechanical characteristics, degradability, and release of drug characteristics. Furthermore, natural high-polymer substances like alginate (AG) and chitosan (CS) have excellent elasticity and permeability [10, 11]. Furthermore, chitosan possesses antibacterial and anti-inflammatory effects that are wide-ranging. It demonstrated excellent bactericidal activity against a variety of oral infections and reduced the development of chronic periodontitis.

The synergistic combination of chitosan (CS), alginate (AG), and substituted hydroxyapatite (SHA) for periodontal tissue regeneration is what makes this study innovative. Although SHA has good biocompatibility and osteoconductivity, especially when co-substituted with strontium and zinc, its limitations in terms of mechanical characteristics, degradability, and drug release may prevent the best possible tissue regeneration [12, 13]. By using the beneficial qualities of chitosan and alginate, this research overcomes these drawbacks [14, 15]. By combining the elasticity and permeability of alginate with the antibacterial and anti-inflammatory properties of chitosan, a composite scaffold may be able to overcome the drawbacks of each component alone [16,17]. By combining the improved mechanical qualities, controlled degradation, and increased biological activity offered by the addition of alginate and chitosan with the structural support and osteoconductivity of SHA, this tri-component scaffold presents a promising strategy to improve periodontal regeneration. A more efficient and adaptable platform for periodontal tissue engineering might be produced by this innovative combination.

This is the first time alginate/chitosan with substituted hydroxyapatite (AG/CS/SHA) has been used in periodontal regeneration. The purpose of this study was to explore the physicochemical characteristics, biocompatibility, and development of human periodontal ligament cells (HPDLCs) in an AG/CS/SHA composite. Furthermore, the AG/CS/SHA composite was implanted in a canine model with periodontal disorders to assess regeneration capacity.

MATERIALS AND METHODS

Preparation of substituted hydroxyapatite

A calcium-zinc-strontium phosphate material was synthesized using a sol-gel method. The precursors employed were calcium nitrate tetrahydrate ($Ca(NO_3)_2{\cdot}4H_2O$), zinc nitrate hexahydrate ($Zn(NO_3)_2{\cdot}6H_2O$), strontium nitrate hexahydrate ($Sr(NO_3)_2{\cdot}6H_2O$), and ammonium phosphate ($(NH_4)_2HPO_4$). Aqueous solutions of the respective metal ions were prepared with the following molar concentrations: 0.9 M calcium, 0.05 M zinc, 0.05 M strontium, and 0.6 M phosphate. In the initial synthesis stage, zinc and strontium solutions were meticulously added dropwise to the calcium solution under simultaneous sonication at room temperature. Following a 15-minute stirring period, the pH of the combined solution was adjusted to 10 through the addition of ammonium hydroxide solution. Subsequently, the ammonium phosphate solution was slowly introduced to this metal ion mixture, resulting in the formation of a precipitate. The precipitated product was then purified through repeated rinsing cycles using deionized water and methanol. The rinsed

precipitate was subsequently dried in an oven at 100 °C for 12 hours. Finally, the dried material was calcined under an argon atmosphere at 500 °C for 8 hours, using controlled heating and cooling rates of 5-10 °C/min, to yield the final SHA product. The phase purity and crystallinity of the synthesized material were confirmed by Fourier Transform Infrared Spectroscopy (FTIR) and X-ray Diffraction (XRD) for subsequent use in the preparation of an Ag/CS/SHA composite.

Preparation of biocomposite

Biocomposite scaffolds composed of alginate (AG), chitosan (CS), and substituted hydroxyapatite (SHA) were fabricated using a freeze-drying technique. Chitosan (2% w/v) was initially dissolved in 20 mL of a 1% acetic acid (CH3COOH) solution. Subsequently, sodium alginate (2% w/v) was added to the chitosan solution, and the mixture was sonicated at room temperature for 30 minutes to ensure homogeneity. For the SHA-containing scaffolds, 3% (w/v) SHA was then incorporated into the homogeneous AG/CS solution and sonicated for an additional 30 minutes. Control scaffolds consisting of only AG and CS were prepared following the same procedure, omitting the SHA addition. Following preparation, the solutions were transferred to culture plates and frozen overnight at -60°C. The frozen samples were then lyophilized (LGJ-10 freeze dryer) for 48 hours at a vacuum pressure of 20 Pa and a cold well temperature of -60°C. Prior to lyophilization, the samples were rinsed three times with deionized (DD) water. The resulting dried composite scaffolds were stored in sealed jars for further analysis.

Characterization

The FTIR analysis was performed on prepared samples using a Bruker Vertex FTIR spectrometer, with a spectral range of 4000 to 500 cm-1. The crystallinity of the prepared samples was determined using a Rigaku D/Max2500VB2 + /Pc diffractometer (Rigaku Company, Tokyo, Japan) with Cu Kα radiation (λ= 0.154nm) at 40 kV and 50mA. The samples were scanned over a 2θ range of 10°-80° at a scanning rate of 5°/min.

Scanning electron microscopy (SEM) was used to examine and characterize the prepared samples. Samples underwent critical point drying with a SANDRI 795 and were then sputter-coated with gold. Images were obtained with a JEOL-JSM6490LV microscope at an accelerating voltage of 10 kV. Pore size was quantified using the FIJI image processing program. Three specimens of each scaffold type were examined. High-resolution transmission electron microscopy (HRTEM) using a JEOL-JEM2100 microscope at 200 kV was used to investigate the internal structure and characteristics.

Swelling studies

The degree of swelling was measured using the traditional gravimetric procedure [18]. The tests were carried out by taking before-weighed specimens and placing them in a Phosphate buffer for 1-7 days before the balanced swelling was achieved. After that the specimens were withdrawn from the solution, pushed between two absorbent paper to dry it and eventually weighed on an electronic scale.

Biodegradability

The biodegradation activities of biocomposites have been tested by weight loss calculation. The biocomposite is immersed in PBS in liquid/solid-lined polyethylene bottles at 37 °C. At the specified periods (1 to 7 days), the samples were taken out. The samples were measured when wet, after cleaning off the surface moisture. They were flushed again with DD water after calculation, dried in a hot air oven at 37 ° C for one day, and assessed accordingly.

MTT assay

The evaluation of cell attachment and proliferation on AG/CS (control) and AG/CS/SHA composite scaffolds was performed using the colorimetric MTT assay. This assay quantifies cellular metabolic activity by measuring the reduction of the yellow tetrazolium salt, MTT, to purple formazan crystals. This reduction is carried out by dehydrogenase enzymes released from the mitochondria of metabolically active cells. The amount of formazan produced is directly proportional to the number of viable cells present. Following the cell culture period, samples were carefully washed with PBS to remove any non-adherent cells. Subsequently, a 20% MTT reagent was added to each well containing the scaffold and cells. The samples were then incubated for 4 hours at 37°C in a humidified atmosphere containing 5% CO2. Finally, the absorbance of the resulting formazan dye was measured at 490 nm using a microplate reader. All MTT assays were performed in triplicate to ensure statistical reliability.

AO/PI dual staining assay

To assess cellular mortality, periodontal ligament stem cells (PDLSCs) were cultured in tissue culture flasks. Following trypsinization, cells were resuspended at a concentration of 1 x 10^5 cells/mL in 200 µL of DMEM supplemented with biocomposites and incubated for 30 minutes.

Subsequently, cells were exposed to 150 µM hydrogen peroxide (H_2O_2) in serum-free DMEM for 20 minutes to induce oxidative stress. Post-treatment, cells were centrifuged at 1200 RPM for 5 minutes, the supernatant was removed, and the cell pellet was resuspended in 10 µL of fresh medium. An equal volume (10 µL) of a dual fluorescent staining solution containing 10 µg/mL acridine orange (AO) and 10 µg/mL propidium iodide (PI) was added to the cell suspension. The stained cells were then transferred onto glass slides, coverslips were applied, and the samples were immediately analyzed using an Olympus BX53 Digital Fluorescence Microscope. Cell counts were performed using ImageJ software with the cell counting plugin. This AO/EB staining procedure was performed in triplicate.

ALP assay

Periodontal ligament cells were cultured in 6-well plates at a density of 4 x 10^5 cells per well to examine the effect of new scaffolds on their alkaline phosphatase (ALP) activity. The control group cells received no treatment (AG/CS), while the experimental group was administered AG/CS/SHA composite scaffolds at a dose of 50 µg/ml. All cultures were sustained at 37°C in a 5% CO_2 environment, with medium supplemented bi-daily. ALP activity, a crucial marker of cellular differentiation and mineralization, was evaluated at one, two, and three weeks with an ALP Assay kit (Sigma-Aldrich). At each time point, cells were collected using 0.25% trypsin-EDTA (Gibco) and enumerated. Aliquots of 2 x 10^4 cells per group were subjected to three washes with PBS to eliminate leftover media and then resuspended in 70 µL of Assay Buffer. To exclude insoluble debris, samples were centrifuged at maximum velocity at 3°C, and the supernatant containing ALP was collected. ALP standards were formulated in accordance with the manufacturer's specifications. For the experiment, 40 µL of a 6 mM pNPP (p-nitrophenyl phosphate) solution was included in each sample and standard, followed by incubation at 27°C for 50 minutes, shielded from light. The reactions were terminated using 25 µL of Stop Solution. Optical density (OD) was measured at 405 nm with a spectrophotometer (Bio-Rad). A standard curve, derived from known ALP values, was used to determine the ALP content in each well. The ALP concentration data for each treatment group was displayed and compared using histograms created using GraphPad Prism. The morphology of the cell monolayer next to the test samples was analyzed using phase-contrast microscopy (Olympus 40×) to assess cellular reactions to the scaffolds.

ARS assay

Alizarin Red S (ARS) staining was performed to assess calcium deposition at one, two, and three weeks. Following two washes with phosphate-buffered saline (PBS), cells in each well were fixed with 300 µL of 10% formalin for 20 minutes. The fixative was then removed by three washes with PBS. Subsequently, the cells were stained for 20 minutes with 300 µL of a freshly prepared 2% ARS solution, adjusted to pH 4.2 using 0.5% ammonium hydroxide. To remove the unbound dye, the cells were washed approximately five times with 1 mL of distilled water per well, continuing until no further dye was visibly released. After the stained cells were allowed to air dry, images were captured using an Olympus inverted microscope.

Statistical analysis

Data are expressed as mean ± standard deviation (SD). Statistical analysis was conducted using one-way ANOVA, succeeded by Tukey's multiple comparison test (GraphPad Prism 8.). Statistical significance was established as $p < 0.05$ ($p < 0.05$, *$p < 0.01$, **$p < 0.001$, ***$p < 0.0001$).

RESULT AND DISCUSSION

Functional group analysis

The FTIR spectra of AG/CS and AG/CS/SHA scaffolds are shown in Fig. 1, which depicts the spectrum of individual elements utilized in scaffold development. The absorption peaks of C-O-C stretching (1022 cm^{-1}) and COO- (1597 cm^{-1}, 1408 cm^{-1}) are clearly seen in the alginate spectra (Fig. 1 a) [18]. As shown in Fig. 1 b, chitosan's typical FTIR spectra emerged at 1645, 1556, 1410, 1375, and 1022 cm^{-1}, referring to amide I, amide II, CH_2 bending, CH_3 symmetrical bending, and C-O-C, respectively [19]. The peaks at 1610 cm-1 sharpened owing to the COO groups in the AG, while the CS amino band at 1596 cm^{-1} vanished, indicating the development of the AG/CS complex (Fig. 1c). A minor peak appeared at about 1080 cm^{-1}, perhaps as a result of ionic interactions between the COH and NH^{3+} groups at the hydrogel surface. The SHA spectra reveal a strong absorption peak at 1019 cm-1, which corresponds to the PO_4^{3-} band, and peaks at 962 cm-1 and 1087 cm^{-1}, which correspond to the P-O stretching (Fig. 1d) [20]. Comparing the FTIR spectrum for AG/CS and AG/CS/SHA composite in Fig.1e clearly indicates the predominance of the interaction between AG/CS and SHA in the ternary composite and the interaction in the ternary composite leads to the distribution of SHA. This report was consistent with previous reports [21, 22].

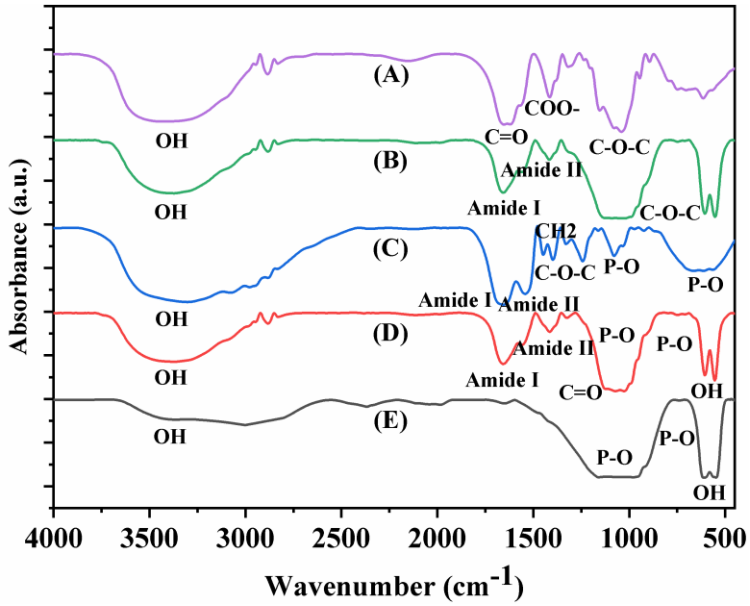

Fig. 1. FT-IR spectra of (A) alginate (B) chitosan, (C) AG/CS (D) SHA and AG/CS/SHA composite (E).

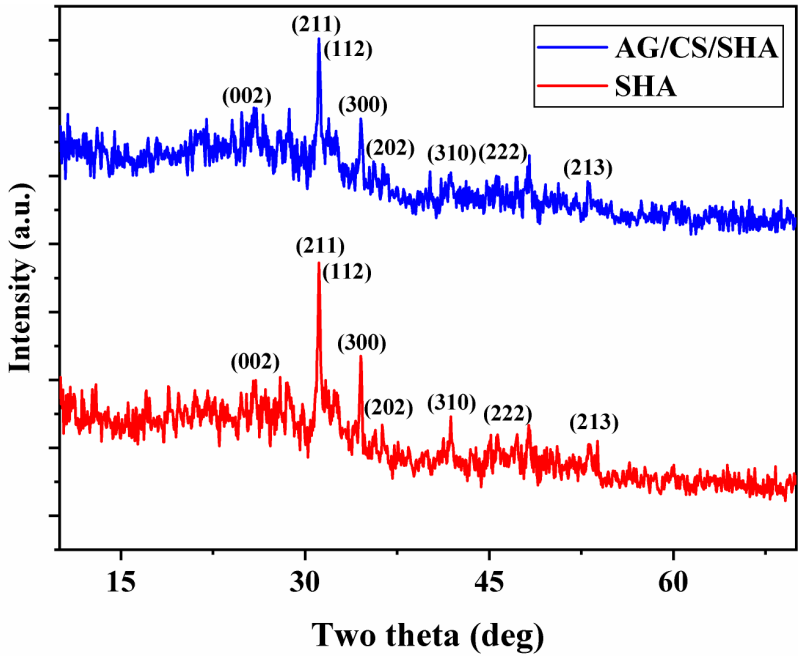

Fig. 2. The XRD patterns of SHA powder (A) and AG/CS/SHA composite (B).

Crystalline structure analysis

The XRD patterns of SHA powder (a) and AG/CS/SHA composite (b) are shown in Fig. 2. For SHA powder, the existence of the diffraction planes of (0 0 2), (2 1 1), (1 1 2), (3 0 0), (2 0 2), (1 3 0), (2 2 2) and (2 1 3) corresponded to the 2 theta bands at 25.8°, 31.8°, 32.1°, 32.9°, 34.0°, 39.9°, 46.7° and 49.4° of the SHA crystallites (Fig. 2a) [23]. The AG/CS/SHA composite displayed alike peaks to the SHA, although the peaks were weaker. The diffraction peaks were affected by the molecular contact between AG/CS and SHA, which resulted in hybridization (Fig. 2b) [24, 25]. The observed diffraction peaks closely match the standard pattern for hydroxyapatite (HA), JCPDS 09-432, confirming the presence of the SHA phase (Ca10(PO4)6(OH)2) within the composite matrix [26, 27].

Morphological analysis

Fig. 3 shows SEM images of different SHA and AG/CS/SHA composites. Fig. 3a, depicts the SHA morphologies of ordered flakes with a width smaller than 250 nm. Because of its similarity to bone minerals, hydroxyapatite (HA), a significant inorganic constituent of bone tissues, is an

attractive contender for bone regeneration scaffold material. In our study, SHA was incorporated into the AG/CS scaffold by generating an AG/CS/SHA composite. Mineral crystals with an even dispersion were found on the scaffold skeleton in the AG/CS/SHA composite. AG/CS/SHA composite has a porous structure with excellent interconnectivity, with pores ranging in size from 100 to 300 µm (Fig. 3b). The size and form of the pores affect the cell's capacity to adhere and develop, therefore affecting the rejuvenation of tissues [28]. As a result, these micropores may enable nutrient and oxygen movement in the composite. The Scanning Electron Microscope (SEM) study demonstrated a porous architecture in the biocomposite, characterized by uniformly distributed tiny particles attributed to the presence of SHA (Fig. 3 B). The pore size of the AG/CS/SHA composite varied between 40 and 60 ± 13 µm. Porous morphology composite scaffolds, like AG/CS/SHA composites, are a significant advancement in bone tissue engineering, especially for dental and orthopedic implant applications [29, 30]. These scaffolds have a highly interconnected porous structure, promoting cell adhesion, proliferation, differentiation, and nutrient and oxygen diffusion. AG and CS offer biocompatibility and biodegradability. Lastly, hydroxyapatite (SHA) mimics the natural mineral composition of bone, enhancing osteoconductivity and mechanical strength [31]. These multifunctional scaffolds not only support bone growth but also address implant challenges like biocompatibility and mechanical stability, making them promising for dental and orthopedic regenerative medicine.

The study using transmission electron microscopy (TEM) revealed the minuscule and complex structure of SHA nanoparticles, with a mean particle size of 55 ± 5 nm. There is a strong correlation between the TEM and SEM pictures of the AG/CS/SHA composite flakes with excellent interconnectivity structures. SAED was used to detect and designate the produced SHA and AG/CS/SHA composite patterns. This pattern matched previously estimated XRD patterns (Fig. 2).

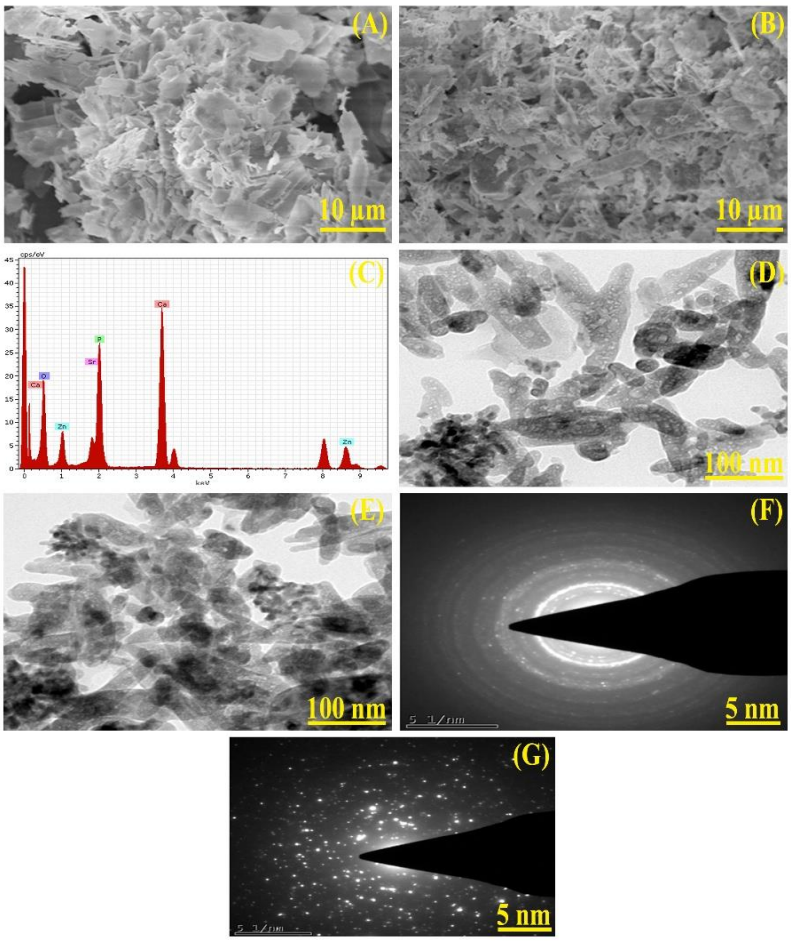

Fig. 3. SEM images of (A) SHA and (B) AG/CS/SHA composite; TEM images of (C) SHA and (d) AG/CS/SHA composite; SAED images of (c) SHA and (d) AG/CS/SHA composite.

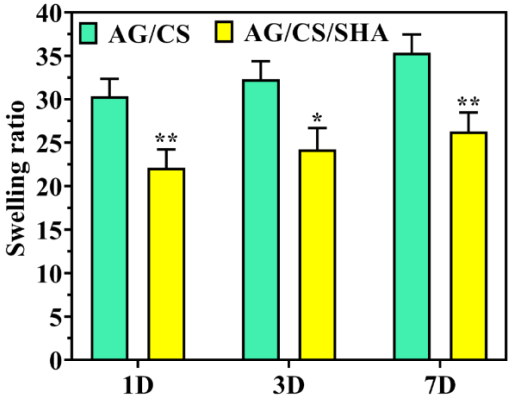

Fig. 4. Swelling studies of AG/CS and AG/CS/SHA composite in PBS medium. Statistical significance was established as *p < 0.01, **p < 0.001, ***p < 0.0001.

Swelling study

Figure 4 (Table S1 in Supplementary file) illustrates the swelling characteristics of the AG/CS and AG/CS/SHA composite scaffolds. SHA-integrated scaffolds had a reduced swelling ratio in comparison to AG/CS control scaffolds. This may be due to the robust interaction between AG/CS and SHA. This may be attributable to the incorporation of SHA, which diminishes pore size. Swelling intensified throughout time until day 7, when the scaffolds commenced degradation. Swelling and porosity facilitate nutrition delivery inside composite scaffolds while enhancing the density for cellular attachment, which is crucial for tissue engineering applications [32]. Conversely, other investigations examining alginate/ chitosan/ gelatine composites with diverse fillers, including titania/hydroxyapatite or other bioceramics, have shown inconsistent swelling tendencies [33, 34].

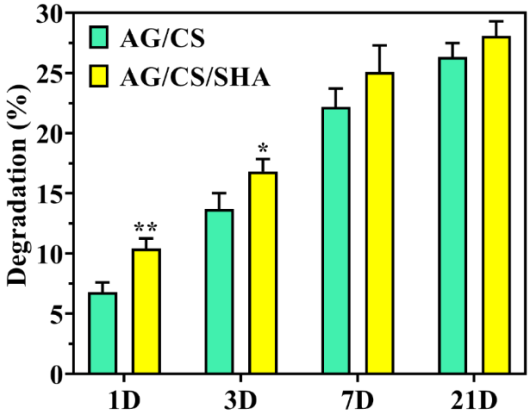

Fig. 5. *In vitro bio*degradation profile of AG/CS and AG/CS/SHA composite in PBS–lysozyme medium. Statistical significance was established as *p < 0.01, **p < 0.001, ***p < 0.0001.

Moreover, research on alginate/chitosan composites including various reinforcing agents, such as graphene oxide (GO) or cellulose nanocrystals (CNC), indicates that the swelling behavior is significantly influenced by the kind and concentration of the filler [35, 36]. The swelling behavior of AG/CS/SHA scaffolds is more regulated than that of other AG/CS-based composites, rendering them appropriate for tissue engineering applications where controlled swelling is essential for preserving mechanical properties and facilitating cell attachment and nutrient delivery. The regulated swelling, together with the bioactive characteristics of SHA, establishes AG/CS/SHA composites as viable options for biomedical applications, especially in bone tissue engineering.

Biodegradability study

In vitro biodegradation investigations Fig. 5 (Table S2 in Supplementary file), demonstrated unique degradation trends for AG/CS and AG/CS/SHA composite scaffolds. The AG/CS/SHA composites demonstrated a somewhat elevated initial degradation rate relative to AG/CS scaffolds up to day 14, likely due to the preferential dissolution of inorganic constituents inside the SHA particles. A significant reduction in the deterioration rate of AG/CS/SHA composites was reported post-day 21. The reduced degradation rate is likely due to the incorporation of SHA inside the matrix and the establishment of ionic cross-links with Ca^{2+} ions, enhancing scaffold durability [37].

The obtained biodegradation patterns indicate that AG/CS/SHA composites have regulated and adjustable degradation characteristics. The initial elevated degradation rate of AG/CS/SHA composites, followed by a notable decline, suggests a capacity for the regulated release of bioactive agents and a progressive degradation pattern that aligns with tissue regeneration timeframes [38, 39]. The regulated degradation behavior is essential for effective tissue engineering applications, as it enables the scaffold to provide structural support during the early phases of tissue creation and then progressively dissolve as the newly developed tissue grows. The results indicate that AG/CS/SHA composites have favorable biodegradation properties, making them suitable for diverse tissue engineering applications.

Cell viability assay

The viability of PDLF in each of the two groups was greater than 90 percent. The proliferation rate of PDLF was investigated using a MTT test during a 7-day period (Fig. 6A). The cell population in the

two groups rose consistently over the course of seven days, with no notable variations between them at any stage. These findings suggest that AG/CS/SHA had no effect on the viability and multiplication of PDLF. Phase contrast microscopy demonstrated a time-dependent enhancement in cell spreading on both AG/CS and AG/CS/SHA biocomposites from 1 to 7 days post-seeding (Fig. 6B). Comparative research revealed that cells showed increased proliferation on the biocomposites relative to the control. The noted increase in cell spreading and proliferation on the biocomposites indicates that these materials provide a favorable environment for cell development. The integration of SHA into the AG/CS matrix likely augments its bioactivity, perhaps via mechanisms such as increased surface roughness, greater protein adsorption, and the liberation of bioactive compounds [40]. The observed increase in cell proliferation corresponding to elevated SHA concentration further substantiates this notion. The outstanding cytocompatibility shown by the MTT experiment signifies that the biocomposites are biocompatible and do not provoke considerable cytotoxicity to the PDLF cells. The results indicate that AG/CS/SHA biocomposites are promising for several biological applications, especially those necessitating cell proliferation and tissue regeneration.

The research underscores the benefits of AG/CS/SHA biocomposites compared to other biomaterials, including synthetic polymers and non-sulfated polysaccharides, regarding bioactivity and cytocompatibility [41, 42]. In contrast to synthetic polymers such as PLGA, which often need surface changes to enhance cellular contact, the inherent characteristics of AG, CS, and SHA make them more suitable for biological applications. The results correspond with other studies, highlighting the promise of these biocomposites in tissue engineering and regenerative medicine. The integration of SHA augments the bioactivity of the AG/CS matrix, facilitating cell proliferation and tissue regeneration.

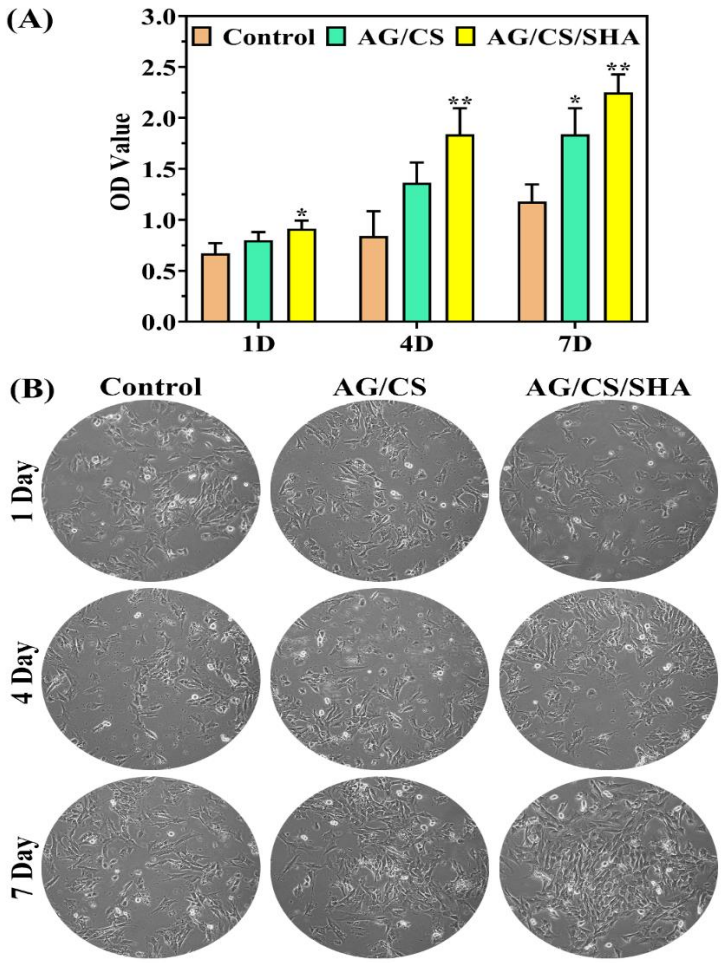

Fig. 6. (A) Assessment of PDLF cell growth rate through MTT assay conducted over a period of 7 days. (B) Images from the phase contest showcasing various samples taken on different days.
* Statistical significance was established as *p < 0.01, **p < 0.001, ***p < 0.0001.

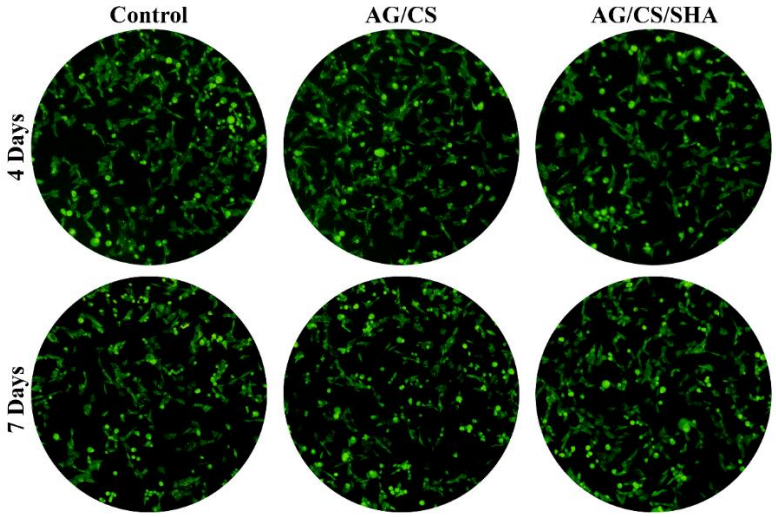

Fig. 7. Live/dead staining of PDLF cells cultured on various samples for 4 and 7 days.

Live /dead assay

Fluorescent microscopy pictures of scaffolds stained with Acridine Orange/Propidium Iodide (AO/PI) were evaluated to evaluate cell viability over time (Fig. 7). Following a 7-day culture period, both the AG/CS and AG/CS/SHA groups had a marginal increase in cell mortality, as shown by red fluorescence. This indicates that while these scaffolds initially facilitate cell development, they may possess constraints for long-term cell survival. The breakdown rate of the scaffolds or the production of degradation products may contribute to this diminished viability. Conversely, the ALG/CS/SHA samples exhibited markedly improved biocompatibility, as shown by an increased percentage of viable cells. The exceptional performance is due to the synergistic effects of ALG, CS, and SHA. ALG, a natural polysaccharide, offers a biocompatible and biodegradable framework, while CS enhances cell adhesion and proliferation [43-45]. SHA, a bioactive ceramic, liberates vital ions for bone mineralization, hence increasing the scaffold's bioactivity [46, 47]. The amalgamated characteristics of these components provide an optimal milieu for cellular development, proliferation, and differentiation, resulting in enhanced cell viability and tissue regeneration.

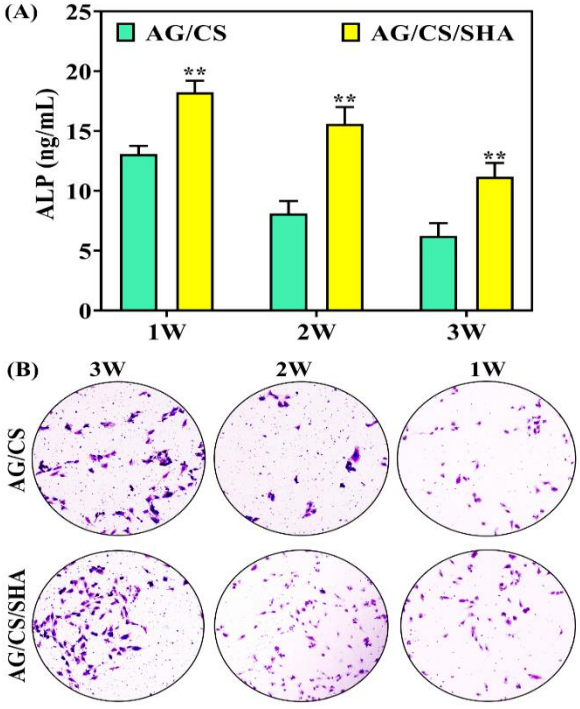

Fig. 8. ALP activity: (A) quantitative investigation. (B) ALP staining images of PDLF cell cultured on AG/CS and AG/CS/SHA composite. Statistical significance was established as *p < 0.01, **p < 0.001, ***p < 0.0001.

Alkaline phosphatase activity

ALP activity analysis revealed an initial increase in PDLF cells cultured on AG/CS/SHA composite scaffolds in 1st week, followed by a decline at 2-3 weeks (Fig. 8). This biphasic pattern is consistent with osteoblastic differentiation, where ALP activity peaks during the early stages of mineralization and subsequently decreases as cells mature and matrix mineralization progresses. Previous studies have reported similar ALP activity profiles in scaffolds for regenerative medicine applications. The addition of SHA to the AG/CS composite significantly enhanced ALP activity compared to the control AG/CS scaffold. This can be attributed to the bioactive nature of SHA, which releases ions and soluble compounds that stimulate osteogenic gene expression and accelerate bone formation. Optical microscopy images of scaffolds stained with ALP further corroborated these findings (Fig. 8B). Intense staining was observed on all composite scaffolds at 1-2 weeks, indicating significant ALP activity during the early stages of mineralization. The reduced staining intensity at 3 weeks aligns with the expected decline in ALP activity as osteoblasts mature and mineralization progresses [48, 49].

Mineralization assay

Optical microscope pictures of scaffolds stained with Alizarin Red S (ARS) were examined to evaluate mineralization over time (Fig. 9). One to two weeks post-implantation, all samples had varied levels of mineralization, as shown by the presence of white regions signifying calcium phosphate deposition. Nevertheless, the ALG/CS sample exhibited much fewer white regions than the ALG/CS/SHA samples, indicating decreased mineral deposition at this initial phase. A further analysis of the photos indicated that ALG/CS/SHA samples had more mineral deposition on their surfaces in comparison to ALG/CS samples at the 1–2-week mark. The ALG/CS/SHA samples had a pronounced red hue, indicating substantial calcium accumulation. The results indicate that the inclusion of SHA into the ALG/CS scaffold improves mineralization and facilitates bone graft integration. A comparison examination was performed between ALG/CS and undifferentiated samples at three weeks post-implantation to reinforce these conclusions. The ALG/CS scaffold demonstrated a significant increase in mineralization, as shown by the pronounced red staining. This outcome highlights the capability of the ALG/CS/SHA scaffold to expedite bone regeneration and tissue healing.

The study highlights the enhanced mineralization observed in ALG/CS/SHA composite scaffolds, attributed to the synergistic effects of alginate (ALG), chitosan (CS), and Zinc-strontium hydroxyapatite (SHA). ALG's biocompatibility and biodegradability, CS's ability to promote cell adhesion and mineral deposition, and SHA's release of calcium and phosphate ions Zinc-strontium collectively create an optimal environment for bone tissue repair [50, 51]. The findings align with existing literature on the importance of mineralization in bone regeneration and the benefits of composite scaffolds in tissue engineering. Notably, the addition of SHA significantly boosts mineralization due to the bioactive properties of zinc and strontium ions. The results suggest that ALG/CS/SHA scaffolds can effectively enhance bone regeneration, with implications for improved clinical outcomes in bone repair. Future studies should explore the long-term effects of these scaffolds in vivo and their potential use in load-bearing.

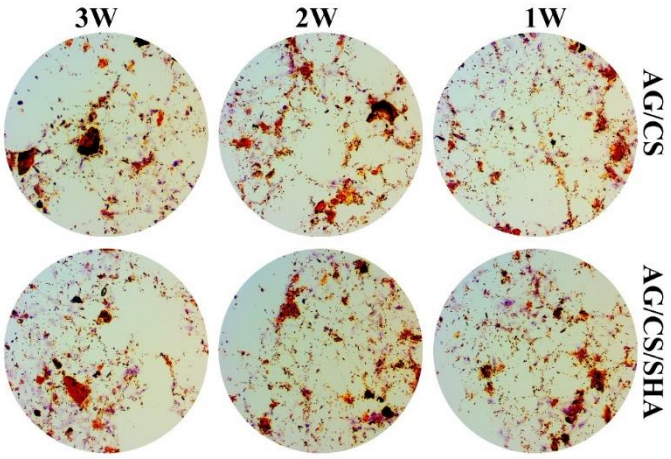

Fig. 9. Microscopy images showcasing ARS staining related to mineralization in PDLF cells over a period from day 1 to 3 weeks.

The physicochemical and biological results from the ALG/CS/SHA scaffold investigation indicate substantial therapeutic significance for bone tissue repair and regeneration. The synergistic interactions of ALG, CS, and SHA provide an ideal environment for mineralization, as shown by increased calcium phosphate deposition and significant calcium accumulation in the ALG/CS/SHA samples. ALG offers a biocompatible and biodegradable scaffold, CS enhances cell adhesion, proliferation, and mineral deposition, whilst SHA releases vital calcium and phosphate ions required for bone mineralization. These qualities synergistically enhance bone regeneration and tissue healing, as shown by the heightened mineralization and red staining in the ALG/CS/SHA scaffolds relative to ALG/CS alone. This indicates that the ALG/CS/SHA scaffold may function as a superior biomaterial for bone grafts, facilitating enhanced integration and expedited healing in orthopedic and dentistry contexts, hence diminishing recovery durations and improving patient outcomes.

CONCLUSION

This work effectively fabrication and characterized a new AG/CS/SHA composite scaffold infused with zinc and strontium-substituted hydroxyapatite (SHA) for applications in bone tissue engineering. The scaffold exhibited a porous, interconnected architecture favorable for cell proliferation and nutrient distribution, with regulated swelling and biodegradation characteristics. *In vitro* tests demonstrated higher biocompatibility, improved cell proliferation, and markedly elevated ALP activity and mineralization (ARS assay) relative to the AG/CS control. The addition of Zn and Sr in HA enhanced the scaffold's osteogenic capacity, presumably by facilitating cell proliferation, bone formation, and exhibiting antimicrobial properties. The results indicate that the AG/CS/SHA composite, augmented with Zn and Sr in HA, has considerable potential as a biomaterial for bone tissue engineering, especially in periodontal and orthopedic contexts. Although more research, including *in vivo* studies and clinical trials, is required to comprehensively evaluate its effectiveness and safety, this new scaffold presents a promising foundation for future progress in regenerative medicine. The possibility for optimization via new production processes, the integration of supplementary bioactive compounds, and the examination of alternative growth factors further substantiates the argument for further research into this intriguing biomaterial.

ACKNOWLEDGEMENT

The authors thank Periyar University for research support, especially for SEM microanalysis.

FUNDING

No funding was received.

AVAILABILITY DATA AND MATERIALS

Data will be provided upon request.

ETHICAL CONSIDERATIONS

This article does not contain any studies on human or animals.

CONFLICT OF INTEREST

There are no potential conflicts of interest.

REFERENCES

1. Chen H, Song G, Xu T, Meng C, Zhang Y, Xin T, Yu T, Lin Y, Han B. Biomaterial Scaffolds for Periodontal Tissue Engineering. J Funct Biomater. 2024;15(8):233.
2. Stefańska K, Volponi AA, Kulus M, Waśko J, Farzaneh M, Grzelak J, Azizidoost S, Mozdziak P, Bukowska D, Antosik P, Zabel M. Dental pulp stem cells–A basic research and future application in regenerative medicine. Biomed. Pharmacother. 2024;178:116990.
3. Wang X, Li H, Mu M, Ye R, Zhou L, Guo G. Recent development and advances on polysaccharide composite scaffolds for dental and dentoalveolar tissue regeneration. Polym Rev. 2025;65(1):47-103.
4. Liu JH, Bian H, Zhang Y, Long Y, Li C, Zhang R, Mao Z, Wu H, Li B, Zhi C, Lu J. Formation of Stable Zinc-Rich Amorphous Calcium Phosphate. Cryst. Growth Des. 2024 Nov 4;24(22):9492-9501.
5. Wang CY, Chen CY, Chen KH, Lin YH, Yeh TP, Lee AK, Huang CC, Shie MY. The synergistic effects of strontium/magnesium-doped calcium silicate cement accelerates early angiogenesis and bone regeneration through double bioactive ion stimulation. Ceram Int. 2024;50(4):7121-31.
6. Olgun O, Gül ET, Kılınç G, Gökmen F, Yıldız A, Uygur V, Sarmiento-García A. Comparative Effects of Including Inorganic, Organic, and Hydroxy Zinc Sources on Growth Development, Egg Quality, Mineral Excretion, and Bone Health of Laying Quails. Biol Trace Elem Res. 2024:1-10.
7. Nadhiya D, Kala A, Sandhiya V, Thirunavukkarasu P, Karnan C, Prabhaharan M, Sasikumar P, Albukhaty S, Sulaiman GM. Influence of annealing temperature on structural, morphological, optical, magnetic, and antimicrobial properties of zinc ferrite nanoparticles. Plasmonics. 2024;19(4):1753-63.
8. Lu T, Miao Y, Wu T, Ye J, Zhang Y. Effects of Zn/Sr co-substitution on the physicochemical properties and cellular responses of wollastonite. Ceram Int. 2024; 50(10):17214-17227.
9. Robinson L, Salma-Ancane K, Stipniece L, Meenan BJ, Boyd AR. The deposition of strontium and zinc Co-

substituted hydroxyapatite coatings. J Mater Sci: Mater Med. 2017;28:1-4.
10. Hanh NT, Bich PT, Thao HT. Acute and subchronic oral toxicity assessment of calcium hydroxyapatite-alginate in animals. Vietnam J Chem. 2019;57(1):16-20.
11. Thang DX, Chinh NT, Ngoc DH, Tung NQ, Hoang T. Effects of processing conditions on properties and morphology of chitosan/lovastatin particles. Vietnam J Chem. 2019;57(1):85-89.
12. Naruphontjirakul P, Li M, Boccaccini AR. Strontium and Zinc Co-Doped Mesoporous Bioactive Glass Nanoparticles for Potential Use in Bone Tissue Engineering Applications. Nanomater. 2024;14(7):575.
13. Vijayakumar G, Sundaram GA, Mani SP, Kumar SP, Krishnan M, Lakshmanan S. Strontium and Zinc doped hydroxyapatite coating on stainless steel mini-implants used in maxillofacial surgery: An in-vitro study. Lib Pro. 2024; 44(3):1846-52.
14. Elkhenany H, Soliman MW, Atta D, El-Badri N. Innovative Marine-Sourced Hydroxyapatite, Chitosan, Collagen, and Gelatin for Eco-Friendly Bone and Cartilage Regeneration. J Biomed Mater Res Part A. 2025; 113(1):e37833.
15. Costa WB, Félix Farias AF, Silva-Filho EC, Osajima JA, Medina-Carrasco S, Del Mar Orta M, Fonseca MG. Polysaccharide hydroxyapatite (nano) composites and their biomedical applications: An overview of recent years. ACS Omega. 2024;9(28):30035-70.
16. Kudiyarasu S, Perumal MK, Renuka RR, Natrajan PM. Chitosan composite with mesenchymal stem cells: Properties, mechanism, and its application in bone regeneration. Int J Biol Macromol. 2024;275:133502.
17. Ren Y, Wang Q, Xu W, Yang M, Guo W, He S, Liu W. Alginate-based hydrogels mediated biomedical applications: A review. Int J Biol Macromol. 2024; 279: 135019.
18. Shavandi A, Bekhit AE, Ali MA, Sun Z, Gould M. Development and characterization of hydroxyapatite/β-TCP/chitosan composites for tissue engineering applications. Mater Sci Eng C. 2015; 56: 481-493.
19. Lawrie G, Keen I, Drew B, Chandler-Temple A, Rintoul L, Fredericks P, Grøndahl L. Interactions between alginate and chitosan biopolymers characterized using FTIR and XPS. Biomacromolecules. 2007;8(8):2533-41.
20. Haghighi M, Yazdanpanah S. Chitosan-based coatings incorporated with cinnamon and tea extracts to extend the fish fillets shelf life: validation by FTIR spectroscopy technique. J Food Qual. 2020; 2020(1): 8865234.
21. Li Z, Saravanakumar K, Yao L, Kim Y, Choi SY, Yoo G, Keon K, Lee CM, Youn B, Lee D, Cho N. Acer tegmentosum extract-mediated silver nanoparticles loaded chitosan/alginic acid scaffolds enhance healing of E. coli-infected wounds. International Int. J Biol Macromol. 2024;267:131389.
22. Anaya-Sampayo LM, García-Robayo DA, Roa NS, Rodriguez-Lorenzo LM, Martínez-Cardozo C. Platelet-rich fibrin (PRF) modified nano hydroxyapatite/chitosan/gelatin/alginate scaffolds increase adhesion and viability of human dental pulp stem cells (DPSC) and osteoblasts derived from DPSC. International Int J Biol Macromol. 2024:133064.
23. Kumar KV, Subha TJ, Ahila KG, Ravindran B, Chang SW, Mahmoud AH, Mohammed OB, Rathi MA. Spectral characterization of hydroxyapatite extracted from Black Sumatra and Fighting cock bone samples: A comparative analysis. Saudi J. Biol. Sci. 2021;28(1):840-846.
24. Abou Taleb MF, Alkahtani A, Mohamed SK. Radiation synthesis and characterization of sodium alginate/chitosan/hydroxyapatite nanocomposite hydrogels: a drug delivery system for liver cancer. Polym Bull. 2015;72:725-42.
25. Liu H, Cui X, Lu X, Liu X, Zhang L, Chan TS. Mechanism of Mn incorporation into hydroxyapatite: Insights from SR-XRD, Raman, XAS, and DFT calculation. Chem Geol. 2021;579:120354.
26. Karatas E, Koc K, Yilmaz M, Aydin HM. Characterization and Comparative Investigation of Hydroxyapatite/Carboxymethyl Cellulose (CaHA/CMC) Matrix for Soft Tissue Augmentation in a Rat Model. ACS omega. 2024 Jul 12;9(29):31586-600.
27. Abdian N, Zangbar HS, Etminanfar M, Hamishehkar H. 3D chitosan/hydroxyapatite scaffolds containing mesoporous SiO2-HA particles: A new step to healing bone defects. Int J Biol Macromol. 2024;278:135014.
28. Perez RA, Mestres G. Role of pore size and morphology in musculo-skeletal tissue regeneration. Mater Sci Eng C. 2016;61:922-939.
29. Monmaturapoj N, Uanlee T, Nampuksa K, Kasiwat A, Makornpan C. Preparation and properties of porous biphasic calcium phosphate/bioactive glass composite scaffolds for biomedical applications. Mater Today Commun. 2022;33:104993.
30. Gritsch L, Perrin E, Chenal JM, Fredholm Y, Maçon AL, Chevalier J, Boccaccini AR. Combining bioresorbable polyesters and bioactive glasses: Orthopedic applications of composite implants and bone tissue engineering scaffolds. Appl Mater Today. 2021;22:100923.
31. Abere DV, Ojo SA, Oyatogun GM, Paredes-Epinosa MB, Niluxsshun MC, Hakami A. Mechanical and morphological characterization of nano-hydroxyapatite (nHA) for bone regeneration: A mini review. Biomed Engineer Adv. 2022;4:100056.
32. Peter M, Kumar PT, Binulal NS, Nair SV, Tamura H, Jayakumar R. Development of novel α-chitin/nanobioactive glass ceramic composite scaffolds for tissue engineering applications. Carbohydr Polym. 2009;78(4):926-31.
33. Chen X, Wang H, Sun X, Bu Y, Yan H, Lin Q. Chemical characterization and biological properties of titania/hydroxyapatite-promoted biomimetic alginate-chitosan-gelatin composite hydrogels. Ceram Int. 2023;49(15):25744-25756.

34. Chen X, Wu T, Bu Y, Yan H, Lin Q. Fabrication and biomedical application of alginate composite hydrogels in bone tissue engineering: A review. Int J Mol Sc. 2024; 25(14):7810.
35. Kolanthai E, Sindu PA, Khajuria DK, Veerla SC, Kuppuswamy D, Catalani LH, Mahapatra DR. Graphene oxide—a tool for the preparation of chemically crosslinking free alginate–chitosan–collagen scaffolds for bone tissue engineering. ACS Appl Mater Interfaces. 2018;10(15):12441-12452.
36. Shaheen TI, Montaser AS, Li S. Effect of cellulose nanocrystals on scaffolds comprising chitosan, alginate and hydroxyapatite for bone tissue engineering. Int J Biol Macromol. 2019;121:814-821.
37. Thai NL, Beaman HT, Perlman M, Obeng EE, Du C, Monroe MB. Chitosan poly (vinyl alcohol) methacrylate hydrogels for tissue engineering scaffolds. ACS Appl Bio Mater. 2024;7(12):7818-7827.
38. Wang F, Cai X, Shen Y, Meng L. Cell–scaffold interactions in tissue engineering for oral and craniofacial reconstruction. Bioact Mater. 2023;23:16-44.
39. Dhivya S, Saravanan S, Sastry TP, Selvamurugan N. Nanohydroxyapatite-reinforced chitosan composite hydrogel for bone tissue repair in vitro and in vivo. J Nanobiotechnology. 2015;13:1-3.
40. Abbass MM, El-Rashidy AA, Sadek KM, Moshy SE, Radwan IA, Rady D, Dörfer CE, Fawzy El-Sayed KM. Hydrogels and dentin–pulp complex regeneration: from the benchtop to clinical translation. Polymers. 2020;12(12):2935.
41. Reddy MS, Ponnamma D, Choudhary R, Sadasivuni KK. A comparative review of natural and synthetic biopolymer composite scaffolds. Polymers. 2021;13(7):1105.
42. Maadani AM, Salahinejad E. Performance comparison of PLA-and PLGA-coated porous bioceramic scaffolds: Mechanical, biodegradability, bioactivity, delivery and biocompatibility assessments. Journal of Controlled Release. 2022;351:1-7.
43. Ghahremani-Nasab M, Akbari-Gharalari N, Rahmani Del Bakhshayesh A, Ghotaslou A, Ebrahimi-Kalan A, Mahdipour M, Mehdipour A. Synergistic effect of chitosan-alginate composite hydrogel enriched with ascorbic acid and alpha-tocopherol under hypoxic conditions on the behavior of mesenchymal stem cells for wound healing. Stem cell res. ther. 2023;14(1):326.
44. Nazemoroaia M, Bagheri F, Mirahmadi-Zare SZ, Eslami-Kaliji F, Derakhshan A. Asymmetric natural wound dressing based on porous chitosan-alginate hydrogel/electrospun PCL-silk sericin loaded by 10-HDA for skin wound healing: In vitro and in vivo studies. Inter J Pharm. 2025;668:124976.
45. He J, Hu X, Cao J, Zhang Y, Xiao J, Chen D, Xiong C, Zhang L. Chitosan-coated hydroxyapatite and drug-loaded polytrimethylene carbonate/polylactic acid scaffold for enhancing bone regeneration. Carbohydr Polym. 2021;253:117198.
46. Rh. Owen G, Dard M, Larjava H. Hydoxyapatite/beta-tricalcium phosphate biphasic ceramics as regenerative material for the repair of complex bone defects. J Biomed Mater Res Part B: Appl Bio Mater. 2018;106(6):2493-2512.
47. Bose S, Tarafder S. Calcium phosphate ceramic systems in growth factor and drug delivery for bone tissue engineering: a review. Acta Biomaterialia. 2012;8(4):1401-1421.
48. Jhundoo HD, Siefen T, Liang A, Schmidt C, Lokhnauth J, Béduneau A, Pellequer Y, Larsen CC, Lamprecht A. Anti-inflammatory activity of chitosan and 5-amino salicylic acid combinations in experimental colitis. Pharmaceutics. 2020;12(11):1038.
49. Kim YB, Kim GH. PCL/alginate composite scaffolds for hard tissue engineering: fabrication, characterization, and cellular activities. ACS Comb Sci. 2015;17(2):87-99.
50. Zhao DW, Liu C, Zuo KQ, Su P, Li LB, Xiao GY, Cheng L. Strontium-zinc phosphate chemical conversion coating improves the osseointegration of titanium implants by regulating macrophage polarization. Chem Eng J. 2021;408:127362.
51. Naruphontjirakul P, Li M, Boccaccini AR. Strontium and Zinc Co-Doped Mesoporous Bioactive Glass Nanoparticles for Potential Use in Bone Tissue Engineering Applications. Nanomater. 2024;14(7):575.